Japanese Journal of Applied Physics **54**, 09MD01 (2015) **REGULAR PAPER**
http://dx.doi.org/**10.7567/JJAP.54.09MD01**

Cell depth imaging by point laser scanning fluorescence microscopy with an optical disk pickup head

Rung-Ywan Tsai*, Jung-Po Chen, Yuan-Chin Lee, Hung-Chih Chiang, Chih-Ming Cheng, Chun-Chieh Huang, Tai-Ting Huang, Chung-Ta Cheng, and Golden Tiao

Biomedical Technology and Device Research Laboratories, Industrial Technology Research Institute, Hsinchu 31040, Taiwan
E-mail: ry_tsai@itri.org.tw

Received December 31, 2014; revised March 21, 2015; accepted March 25, 2015; published online July 29, 2015

A compact, cost-effective, and position-addressable digital laser scanning microscopy (DLSM) instrument is made using a commercially available Blu-ray disc read-only memory (BD-ROM) pickup head. Fluorescent cell images captured by DLSM have resolutions of 0.38 μm. Because of the position-addressable function, multispectral fluorescence cell images are captured using the same sample slide with different excitation laser sources. Specially designed objective lenses with the same working distance as the image-capturing beam are used for the different excitation laser sources. By accurately controlling the tilting angles of the sample slide or by moving the collimator lens of the image-capturing beam, the fluorescence cell images along different depth positions of the sample are obtained. Thus, *z*-section images with micrometer-depth resolutions are achievable.

1. Introduction

Laser scanning confocal microscopy (LSCM) is commonly used for the detection of cell fluorescence.[1,2] The traditional LSCM using an accurate translation stage with a resolution of less than 1 μm is expensive and bulky.[3] In our previous study, we developed a compact, cost-effective, and position-addressable digital laser scanning microscopy (DLSM) instrument using a commercially available Blu-ray disk pickup head (PUH).[4] The PUH comprises two objective lenses with numerical apertures (NAs) of 0.85 and 0.6, which are used to focus blue (405 nm) and red (650 nm) laser beams onto the sample slide, respectively. A specially designed sample slide with sample-holding areas and address-patterned areas for image capture and address recognition, respectively, is used. When the red laser beam is focused onto the address-coded pattern, the blue laser beam is simultaneously focused onto the cell sample. Because the image-capturing and position-recognizing beams are located adjacent to each other and move synchronously, the obtained cell image or the signal of each sampling area has an accurate corresponding address. The resolution of the measured fluorescence image is 0.38 μm, which is determined by the feature size of the address pattern.[4]

In addition to its compact size and low cost, several advantages are expected for the position-addressable DLSM instrument with the commercially available Blu-ray disk PUH. A large-format cell image can be obtained by stitching the small-format images adjacent to each other.[4] The signal-to-noise ratio of the image can be increased by scanning the same address image multiple times to multiply the signal intensity, while the variation of the standard deviation of background noise remains nominal.[5,6] The three-dimensional (3D) image can be obtained by stacking the images measured at different *z*-sections at the same *x*–*y* position.[7–11] The same cell sample stained with different fluorescent dyes can be measured using different wavelengths of excitation laser sources to obtain the multispectral fluorescence image, which is commonly used for the dynamic diagnosis of drug and cell reactions.[12–15] The evolution of disease progression can also be analyzed by time-lapse imaging of the same sample area.[15–18] Meanwhile, the DLSM instrument can potentially be modified to enable integration with a flow cytometer or other biomedical instruments for cell image recognition and differentiation.[19–24]

However, several limitations of the DLSM instrument must be overcome before it can be applied in multispectral fluorescence imaging and *z*-section imaging. The objective lens of the commercial PUH located at the lens holder is optimized for a certain wavelength laser beam. For multi-spectral fluorescence imaging applications, different objective lenses with the same working distance to the same sample slide must be designed and manufactured without changing the construction of the lens holder. To obtain the *z*-section images along the depth, the image-capturing beam must be focused on the various depth positions of the sample, which is easily accomplished by traditional LSCM. However, the displacement of the focal spot of the image-capturing beam in DLSM is confined by the colocation of the two objective lenses and the fixed working distances.[4] The autofocusing of the position-recognizing beam implies that the position of the focal spot of the image-capturing beam is also fixed. Therefore, a way must be found to focus the image-capturing beam onto the different sample depth positions without destroying the autofocusing of the position-recognizing beam.

In this study, we propose solutions to overcome the above-mentioned disadvantages of DLSM. A specially designed objective lens for a 488 nm excitation laser is used. The working distance of the 488 nm objective lens is the same as that of the 405 nm objective lens, whereas the thickness of the 488 nm objective lens is less. Cell samples stained with different fluorescent dyes excited by the 405 and 488 nm laser beams are thus measured by DLSM for multispectral fluorescence analyses. The *z*-section images of the cell are measured by tilting the sample slide using its left-hand edge as a pivot. The distance of sample slide motion relative to the objective lens of the image-capturing beam corresponds to the movement of the focus spot of the image-capturing beam along the depth of the sample. Another way to measure the *z*-section images without tilting the sample is to move the collimator lens of the image-capturing beam to change the front focal length of the objective lens, in which the working distance between the sample slide and the objective lens of

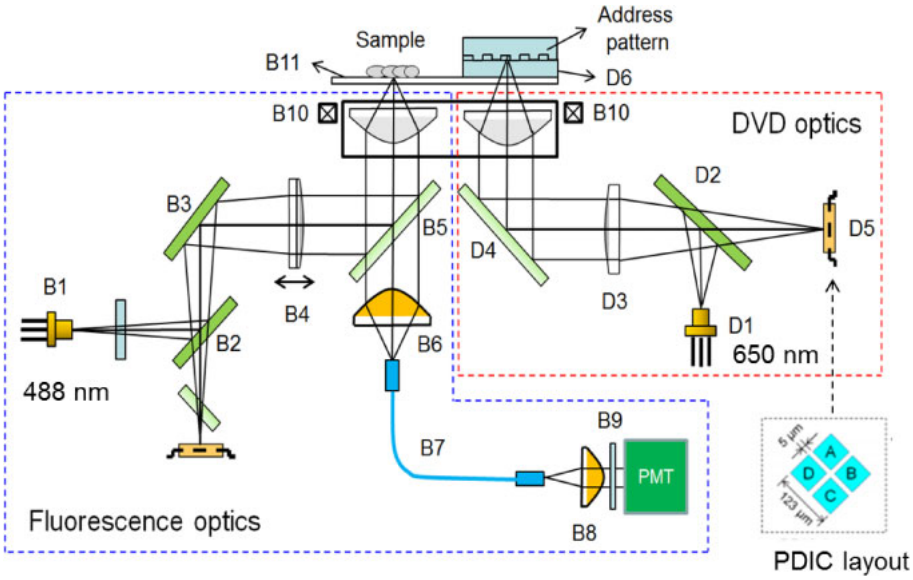

Fig. 1. (Color online) Schematic view of the optical structure of the DLSM instrument with a commercial BD-ROM optical PUH module.

the PUH is fixed. The influences of the tilt angle of the sample slide and the movement of the collimator lens on the z-section images are also investigated.

2. Experimental procedure

A schematic view of the optical structure of the DLSM instrument with a commercial BD-ROM optical PUH module (Sanyo SF-BD412) is shown in Fig. 1. The fluorescence and DVD optics were used for fluorescence cell image capture and sample focusing along with position recognition, respectively. A specially designed objective lens for the image-capturing beam was used to excite the sample stained with Alexa Fluor® 488 phalloidin (Molecular Probes, 30 U/mL), which absorbed the excitation laser of 488 nm and emitted fluorescent light near 519 nm. The working distance of the 488 nm objective lens was 0.36 mm, which was the same as that of the 405 nm objective lens (Fig. 2).[4] The laser beam passed through a 0.074-mm-thick BK7 cover glass and focused on the bottom surface of the cell sample, which was in contact with the cover glass. The quality of the focused beam was checked by a spot checker (Opto Device BSX-001). The measured focus spot size was uniformly distributed in the x–y direction without any obvious coma, and the full-width at half-maximum (FWHM) was 0.33 μm [Fig. 2(b)], which was close to the designed value of 0.36 μm [Fig. 2(a)].[25] The smaller focus spot was probably caused by the spherical aberration of the lens that narrowed the focus beam. Although the focus spot size of the 488 nm image-capturing beam was larger than the 0.26 μm of the 405 nm image-capturing beam, it was still smaller than the feature size of the address-coded pattern (0.38 μm). The focal depth of the 488 nm beam spot determined as two times the Rayleigh length, was about 1.4 μm, which could provide micrometer resolution for the z-section images along the depth of the sample.

A specially designed glass slide with the dimensions of $76.2 \times 25.4 \times 1.1\,\mathrm{mm}^3$ (length × width × height) was used as a sample slide.[4] The sample slide contained eight wells, and each well contained one sample-holding area and one address-patterned area. The gap between the sample-holding area and address-patterned area (Δg) was 4.5 mm, which was equivalent to the distance between the image-capturing and position-recognizing beams. Human-hepatoma-derived (HA22T/VGH) and monkey-derived kidney epithelial (VERO) cells stained with fluorophore phalloidin CF™ 405 and Alexa Fluor® 488 phalloidin, respectively, were seeded on the sample-holding areas for morphological evaluations, and fluorescence cell images were measured by DLSM using 405 and 488 nm excitation laser sources, respectively. Fluorescence images of the cells stained with Alexa Fluor® 488 phalloidin were also measured by LSCM for comparison. No cell images of the sample stained with fluorophore phalloidin CF™ 405 were observed by LSCM because of the lack of a 405 nm excitation laser.

The z-section of the fluorescence cell image was evaluated by tilting the sample slide using its left-hand edge as a pivot (Fig. 3). The tilting distance ΔD at the right-hand edge and the tilt angle θ of the sample slide were controlled manually by inserting a washer with a thickness of ΔD under the bottom of the right-hand edge of the sample slide. The length of the sample slide (L) was 76.2 mm, and the distance between the image-capturing and position-recognizing beams (Δg) was 4.5 mm. When the position-recognizing beam was autofocused onto the servo pattern of the address-coded pattern, the moved distance (Δz) of the focal point of the image-capturing beam along the sample depth direction could be calculated from

$$\Delta z = \frac{\Delta D}{L} \times \Delta \mathrm{g} = \tan\theta \times \Delta \mathrm{g}. \quad (1)$$

According to Eq. (1), the moved distance Δz was 3 μm when the tilting distance ΔD of the sample slide was 0.05 mm.

The z-section of the fluorescence cell image was also evaluated by moving the collimator lens B4 of the image-capturing beam (Fig. 1). The movement in the collimator lens B4 toward the right and left directions was controlled by a stepping motor (Sanyo LB1848MC-AH). The distance of one step of the motor movement was equal to 0.05 mm. The

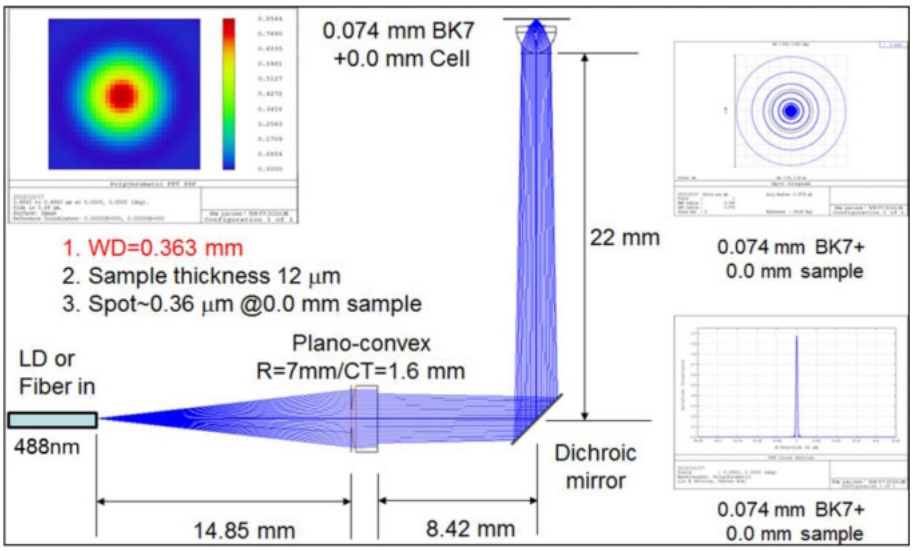

(a)

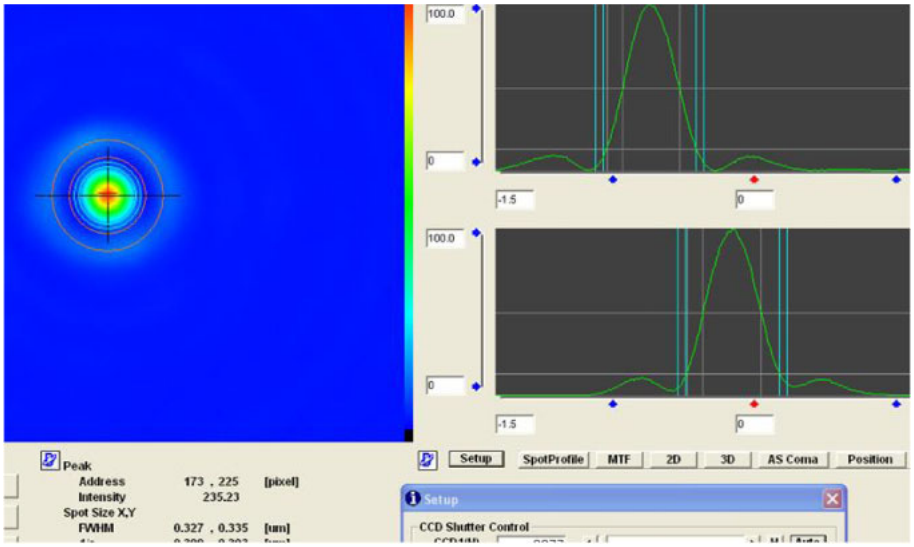

(b)

Fig. 2. (Color online) Optical structure (a) and measured beam spot (b) of the image-capturing beam with a 488 nm excitation laser source.

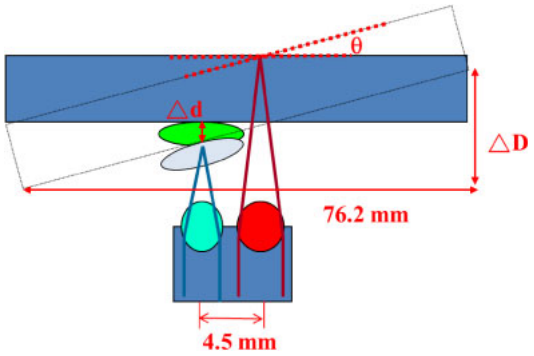

Fig. 3. (Color online) Schematic view of the movement in the focal point of the image-capturing beam along the depth of the sample resulting from the tilting of the sample slide.

moving of B4 changed the front focal length of the image-capturing beam. When B4 moved a distance of 0.05 mm toward the left or right direction, the front focal length of the image-capturing beam increased or decreased by 0.57 μm, respectively. Therefore, the focal point was scanned upward or downward along the sample depth direction by moving the collimator lens B4, and the z-section image was obtained without tilting the sample slide or the objective lens.

3. Results

Fluorescence HA22T/VGH and VERO cell images stained with phalloidin CF™ 405 and Alexa Fluor® 488 phalloidin, respectively, were captured by DLSM (Fig. 4). The control voltage of the PMT was 0.94 V with a gain of 1.13×10^6. Cell images of samples stained with Alexa Fluor® 488 phalloidin and captured by LSCM (Leica TCS SP2) with a 488 nm excitation laser and a NA of 1.4 are included for comparison.[3)] The resolutions of the DLSM fluorescence cell images using the 405 and 488 nm excitation laser sources were 0.38 μm, which were close to that of LSCM images, whereas the contrasts of the cell images measured by DLSM were not as good as that of the LSCM images. The superior contract of the image measured by LSCM is due to the higher NA (1.4) of the objective lens and better confocal config-

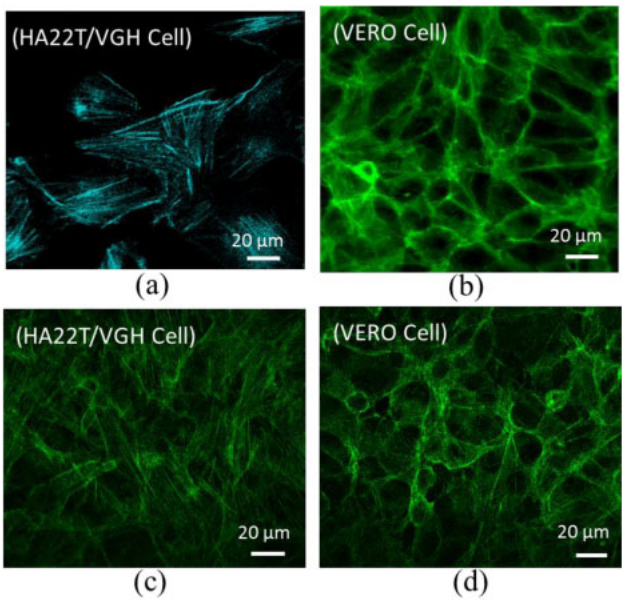

Fig. 4. (Color online) Fluorescence HA22T/VGH (a) and VERO (b) cell images stained with phalloidin CF™ 405 and Alexa Fluor® 488 phalloidin, respectively, and captured by DLSM. Fluorescence HA22T/VGH (c) and VERO (d) cell images stained with Alexa Fluor® 488 phalloidin and captured by LSCM (Leica TCS SP2).

uration than that of DLSM. The optical resolutions of the image capturing beams were 0.26 and 0.33 μm for the 405 and 488 nm laser sources, respectively, which were better than 0.38 μm. The fluorescence signal of the sample was coregistered with the push–pull (PP) signals measured from the address-coded patterns.[4] Therefore, the image resolution of DLSM was limited by the feature size of 0.38 μm of the address pattern in this case. To further improve the image resolution of DLSM, a smaller feature size of the address-coded pattern and a larger NA objective lens should be used. The higher NA values of the objective lenses not only increased the image resolution, but also decreased the noise coming from the other area of the sample, which increased the image contrast.[5]

The z-section VERO cell images were measured by tilting the sample slide using its left-end edge as a pivot (Fig. 5). When the tilted distance ΔD was 0.05 mm, the corresponding moved distance Δz of the focal point of the image-capturing beam along the sample depth was approximately 3 μm, as calculated from Eq. (1). Figure 5 shows that the image measured at $\Delta z = 0$ μm became a little blurry at $\Delta z = 3$ μm. The fine tuning range of the z-section image was determined through accurate control of the tilting distance ΔD and tilt angle θ of the sample slide, by placing a washer with thickness of ΔD under the right-hand edge of the sample slide. For commercial applications, the z-section image could be obtained by tilting the objective lenses instead of the sample slide, which could be easily controlled by the voice coil motor (VCM) of the PUH.[26,27]

Another way of obtaining the z-section cell images without tilting the sample slide was to move collimator lens B4 of the image-capturing beam (Fig. 6). When B4 moved toward the left-hand side, the front focal length of the objective lens of the image-capturing beam increased. The movement of B4 was controlled by a stepping motor. The minimum step of the current stepping motor was 0.05 mm, and the corresponding

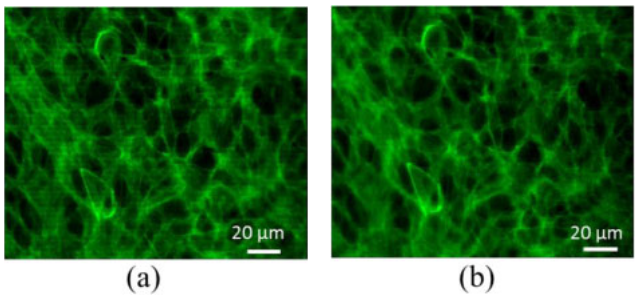

Fig. 5. (Color online) Fluorescence VERO cell images stained with Alexa Fluor® 488 phalloidin and captured by DLSM without (a) and with (b) tilting of the sample slide ($\Delta D = 0.05$ mm).

moved distance in the front focus length of the objective lens of image-capturing beam was 0.57 μm. When B4 moved 1 mm towards the left-hand side, the front focal length of the objective lens of the image-capturing beam was increased by 11.1 μm. The adjustable front focal length of DLSM was ±20 μm without deterioration of the spot quality (simulated Strehl ratio >0.8), being larger than the thickness of a single cell.[5] The fluorescence VERO cell images stained with Alexa Fluor® 488 phalloidin and captured by moving B4 towards the left-hand site at distances of 0, 1, and 2.5 mm are shown in Figs. 6(b), 6(c), and 6(d), respectively; the corresponding moved distances in Δz were 0, 11.1, and 24.9 μm, respectively. The obtained fluorescence cell images started out blurry and then became clear, indicating defocusing and focusing of the image-capturing beam along the sample depth direction.

4. Discussion

To adjust the position of the focus spot of the image-capturing beam relative to the sample depth, the sample slide can be tilted by inserting a washer of a certain thickness, but this is impractical for commercial application. A tilting mechanism within the sample holder is necessary to control the tilting distance ΔD and tilting angle θ. In fact, the tilting of the objective lens holder relative to the fixed sample slide has the same effect as tilting the sample slide relative to the fixed objective lens holder. The tilting of the objective lens holder can be easily controlled by a VCM along the vertical directions.[26,27] The VCM actuator is composed of three magnets (two for focusing and one for tracking) and four wire springs. The tilting and focusing motions of the objective lens holder are caused by the sum of two focusing forces of actuator. If the directions of two forces of the same magnitude are the same, it is a focusing VCM and if the directions are opposite, it acts as a tilting VCM.[28] For example, the auto-focusing of the position-recognizing beam is controlled using the focusing VCM to adjust the vertical distance between the objective lens and the address-coded pattern of the sample slide on the basis of the focus error signal $(A + C) - (B + D)$, where A, B, C, and D are the intensities of the four divided regions of photodetector D5 shown in Fig. 1.[27,29] When the position-recognizing beam is then tracking and autofocusing on the address-coded pattern and the focal point of the image-capturing beam is then moved by a distance Δz along the depth of the sample in accordance with the tilting distance and angle of the objective lenses. The tilting of the objective lens of the image-capturing

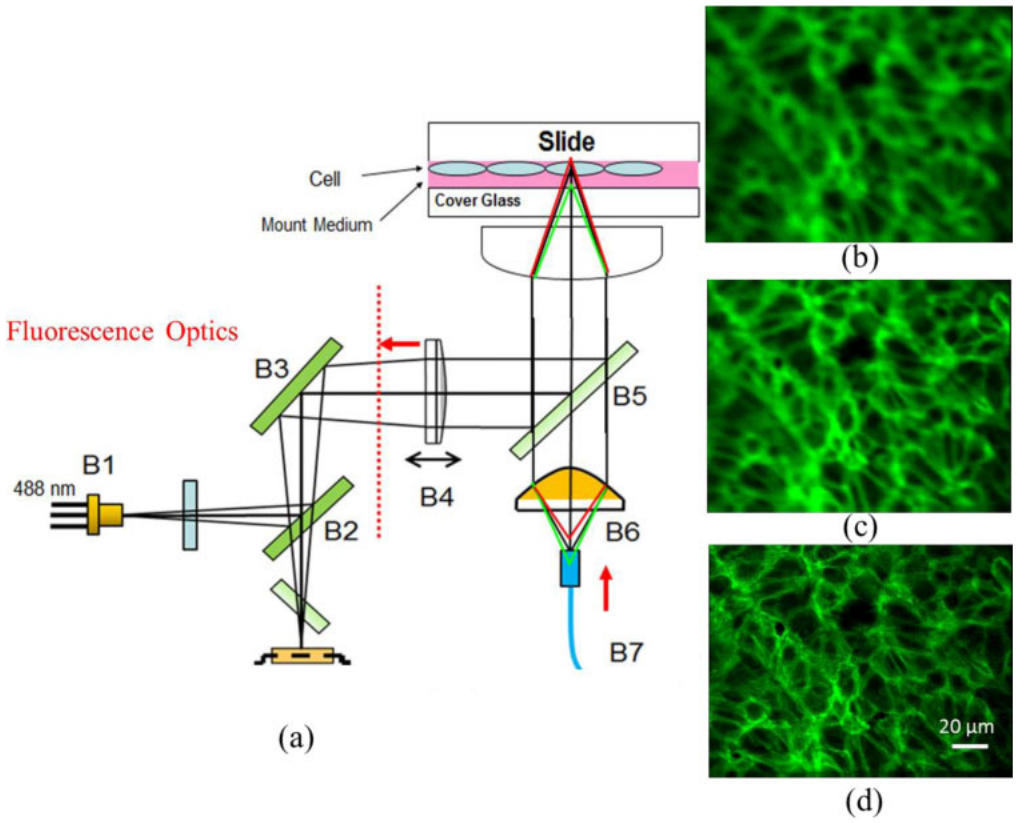

Fig. 6. (Color online) Influence of the movement of B4 on the front focal length of the objective lens of image-capturing beam (a) and fluorescence VERO cell images stained with Alexa Fluor® 488 phalloidin captured by moving B4 towards the left-hand side at distances of 0 (b), 1 (c), and 2.5 mm (d).

beams can be controlled by a tilting VCM, which is easier than tilting the sample slide.

The tilting of the sample slide relative to the optical axis of the objective lens induces coma and astigmatism aberrations and deteriorates the image quality. According to Marechal's criterion, the Strehl ratio of the objective lens after transmission or reflection should be more than 0.8. The calculated root mean square of wavefront aberration is less than 0.07λ.[5] If the overall root mean square of wavefront aberration is larger than 0.07λ, the desired beam spot quality cannot be obtained. When the tilting distance and angle are small, the coma aberration is dominant. In order to avoid the crosstalk caused by coma aberration, the tilt angle θ must be less than 0.013 rad (0.75°) to reduce the deterioration of the image quality.[5] Therefore, according to Eq. (1), the maximum tolerable moved distance Δz of the image-capturing beam is ±29 μm (4.5 tan 0.75° = 0.058 mm), which is large enough to cover the entire thickness of a single cell. However, the scanning of the focus spot of the image-capturing beam along the depth of the sample induces spherical aberration, which is in proportion to about four times the NA of the objective lens. The maximum tolerable moved distance Δz of the image-capturing beam to meet Marechal's criterion is therefore reduced to less than ±7 μm, which is about the same as the thickness of a single cell.

The z-section cell images without tilting the sample slide or objective lenses are obtained by moving collimator lens B4 of the image-capturing beam. However, the variation in the front focal length of the objective lens upon moving B4 also changes the front focal length of focus lens B6. In order to obtain the confocal image, optical fiber B7 acting as a pinhole is moved to the focal point of focus lens B6 of the image-capturing beam (Fig. 6). The moving of optical fiber B7 causes an alignment issue, and an accurate translation stage is needed to hold the position of pinhole B7 at the focal point of B6. In order to avoid increasing the manufacturing cost by using an expensive translation stage, collimator lens D3 of the position-recognizing beam can be moved without moving collimator lens B4 or optical fiber B7 of the image-capturing beam to capture the z-section image. Moving collimator lens D3 changes the front focal length of the objective lens of the position-recognizing beam. Owing to the colocation of the two objective lenses, the autofocusing of the position-recognizing beam leads to an upward or downward movement of the image-capturing beam with a fixed front focal length. Therefore, the focal point of the image-capturing beam is scanned along the depth direction of the sample by moving D3. In this case, the confocal condition of the image-capturing beam is always maintained and no accurate or expensive translation stage is necessary. It could be the most cost-effective and user-friendly method among our proposals.

5. Conclusions

A compact, cost-effective, and position-addressable DLSM instrument was made using a commercially available optical BD-ROM PUH. Owing to the position-addressable function, the system has the potential to be used to collect the multispectral fluorescence and z-section images of cell samples. Because of the colocation of the two objective lenses and the fixed working distances, objective lenses of the image-capturing beams in multispectral fluorescence image

applications have the same working distance for different wavelengths of excitation laser sources. To obtain z-section images, the focus spot along the depth of the sample was moved by tilting the sample slide or objective lenses. Alternatively, the z-section image could be obtained by moving collimator lens B4 of the image-capturing beam; however, an accurate and expensive translation stage must be adopted to capture confocal images. A method without the need to use such an accurate and expensive translation stage for confocal z-section image capturing was also proposed, in which collimator lens D3 of the address-recognizing beam was moved instead of collimator lens B4 of the image-capturing beam. The effect of moving D3 to obtain the z-section image of the cells will be investigated in future studies.

Acknowledgment

We thank the Industrial Technology Research Institute for financial aid provided under project codes D101WBB000 and D101W44100.

1) R. Weissleder and V. Ntziachristos, Nat. Med. **9**, 123 (2003).
2) J. Neauport, P. Cormobard, P. Legros, C. Ambard, and J. Destribats, Opt. Express **17**, 3543 (2009).
3) Web [http://digital.bsd.uchicago.edu/equipment_files/Leica%20SP2%20manual.pdf].
4) R. Y. Tsai, J. P. Chen, Y. C. Lee, C. C. Huang, T. T. Huang, H. C. Chiang, C. M. Cheng, F. H. Lo, S. L. Chang, K. Y. Weng, L. P. Chung, J. C. Chen, and G. Tiao, Biomed. Opt. Express **5**, 427 (2014).
5) K. H. Kim, S. Y. Lee, S. Kim, S. H. Lee, and S. G. Jeong, Microsyst. Technol. **13**, 1359 (2007).
6) G. M. R. De Luca, R. M. P. Breedijk, R. A. J. Brandt, C. H. C. Zeelenberg, B. E. de Jong, W. Timmermans, L. N. Azar, R. A. Hoebe, S. Strallinga, and E. M. M. Manders, Biomed. Opt. Express **4**, 2644 (2013).
7) A. Antonini, C. Liberale, and T. Fellin, Opt. Express **22**, 14293 (2014).
8) J. M. Jabbour, B. H. Malik, C. Olsovsky, R. Cuenca, S. Cheng, J. A. Jo, Y. S. Cheng, J. M. Wright, and K. C. Maitland, Biomed. Opt. Express **5**, 645 (2014).
9) W. R. Zipfel, R. M. Williams, and W. W. Webb, Nat. Biotechnol. **21**, 1369 (2003).
10) G. J. Brakenhoff, G. W. H. Wurpel, K. Jalink, L. Oomen, L. Brocks, and J. M. Zwier, J. Microsc. **219**, 122 (2005).
11) M. Schrader, U. G. Hofmann, and S. W. Hell, J. Microsc. **191**, 135 (1998).
12) H. W. Yang, M. Y. Hua, H. L. Liu, R. Y. Tsai, S. T. Pang, P. H. Hsu, H. J. Tang, T. C. Yen, and C. K. Chuang, Biomaterials **33**, 3919 (2012).
13) S. Srigunapalan, I. A. Eydelnent, C. A. Simmons, and A. R. Wheeler, Lab Chip **12**, 369 (2012).
14) L. W. Zhang and N. A. Monteiro-Riviere, J. Biomed. Opt. **18**, 061214 (2012).
15) J. A. Galeano Z., P. Sandoz, E. Gaiffe, S. Launay, L. Robert, M. Jacquot, F. Hirchaud, J.-L. Prétet, and C. Mougin, Biomed. Opt. Express **2**, 1307 (2011).
16) R. P. J. Barretto, T. H. Ko, J. C. Jung, T. J. Wang, G. Capps, A. C. Waters, Y. Ziv, A. Attardo, L. Recht, and M. J. Schnitzer, Nat. Med. **17**, 223 (2011).
17) Z. Gorocs and A. Ozcan, IEEE Rev. Biomed. Eng. **6**, 29 (2013).
18) A. Kasukurti, M. Potcoava, S. A. Desai, C. Eggleton, and D. W. M. Marr, Opt. Express **19**, 10377 (2011).
19) S. Kostner and M. J. Vellekoop, Sens. Actuators B **132**, 512 (2008).
20) V. Yim, S.-Y. Lee, S. Kim, and J. Y. Park, Proc. IEEE Conf. Engineering in Medicine and Biology Society, 2008, p. 2749.
21) T. Shimomura, C. Izawa, and T. Matsui, Rev. Sci. Instrum. **79**, 035101 (2008).
22) S. Morais, J. Carrascosa, D. Mira, R. Puchades, and A. Maquieira, Anal. Chem. **79**, 7628 (2007).
23) L. Wang and C. H. Lee, Anal. Chim. Acta **687**, 12 (2011).
24) Z. W. Zhong and W. W. Than, Proc. SPIE **4596**, 48 (2001).
25) R. W. Cole, T. Jinadasa, and C. M. Brown, Nat. Protoc. **6**, 1929 (2011).
26) T. Shimomura, C. Izawa, and T. Matsui, Meas. Sci. Technol. **19**, 085404 (2008).
27) J. Benschop and G. V. Rosmalen, Appl. Opt. **30**, 1179 (1991).
28) J. Y. Kang and M. G. Yoon, Proc. American Control Conf., 1998, p. 861.
29) Y. C. Lee, S. Chao, C. C. Huang, and K. C. Cheng, Opt. Express **21**, 23556 (2013).